Quaternary Research (2021), **104**, 170–181
doi:10.1017/qua.2021.15

Research Article

Chronological and rock magnetic constraints on the transition of the Quaternary paleoclimate in the western Qaidam Basin, NE Tibetan Plateau

Weilin Zhang[a,b*], Tao Li[b,c], Xiaomin Fang[a,b], Tao Zhang[d], Maodu Yan[a,b], Jinbo Zan[a,b], Yibo Yang[a,b] and Dhan Bahadur Khatri[b,c]

[a]CAS Center for Excellence in Tibetan Plateau Earth Sciences, Chinese Academy of Sciences (CAS), Beijing 100101, China; [b]CAS Key Laboratory of Continental Collision and Plateau Uplift, Institute of Tibetan Plateau Research, Chinese Academy of Sciences, Beijing 100010, China; [c]University of Chinese Academy of Sciences, Beijing 100049, China and [d]School of Earth Sciences & Key Laboratory of Western China's Mineral Resources of Gansu Province, Lanzhou University, Lanzhou 730000, China

Abstract

A closed Quaternary saline paleolake, currently still a lake and named Dalangtan after one of its largest sub-basins, has widely distributed sediments in the western Qaidam Basin, NE Tibetan Plateau. Lacustrine salt minerals and fine sediments from this paleolake provide an environmental record for investigating paleoclimatic evolution in the Asian interior. However, detailed continuous Pliocene–Quaternary paleoclimatic records are broadly lacking from the NE Tibetan Plateau owing to poor exposure of the outcrops in section. For this study, we performed a detailed magnetostratigraphic dating and rock magnetic analysis on a 590-m-long core from the SG-5 borehole in the western Qaidam Basin. The results demonstrate that the lacustrine sediments in the SG-5 borehole were deposited more than ~3.0 Ma. Saline minerals began to increase at 1.2 Ma, and the magnetic susceptibility (χ) also changed at that time; the percentage frequency-dependent magnetic susceptibility was relatively low and uniform throughout the whole core. These observations, combined with the χ, pollen, salt ion, and grain-size records from other boreholes, indicate that the western Qaidam Basin and the greater Asian interior had a significant climate transition at 1.2 Ma during an extreme drought.

Keywords: Magnetostratigraphy, Rock magnetism, Paleoclimate, Quaternary paleolake, Western Qaidam Basin

(Received 15 September 2020; accepted 17 February 2021)

INTRODUCTION

The most prominent climatic feature in central Asia is Quaternary desertification, such as the formation of the desert, the Yardangs, and the arid inland that covers the westerly dominated mid-latitude areas (Fig. 1; An et al., 2001; Zan et al., 2010; Kapp et al., 2011; Fang et al., 2020). This large east–west longitudinal distribution of arid lands in the Asian interior has long been thought to have a link with global cooling (Kutzbach et al., 1989; Raymo and Ruddiman, 1992; Felzer et al., 1995; Ramstein et al., 1997), the uplift of the Tibetan Plateau (Ruddiman and Kutzbach, 1989; Kutzbach et al., 1993; Molnar et al., 1993; Wang et al., 1999) and its interactions (Wang et al., 1999; An et al., 2001; Dupont-Nivet et al., 2007), and the retreat of the Para-Tethys Sea (Ramstein et al., 1997; Bosboom et al., 2011, 2014).

Irrespective of which mechanism drove the desertification of the Asian interior, Quaternary climates have experienced several significant transitions (Ruddiman and Kutzbach, 1989; Clark et al., 2006; Song et al., 2014). The drying process of central Asia has been recorded in the loess from the western Kunlun Mountains (Zan et al., 2010, 2013), the Tianshan Mountains (Fang et al., 2002; Song et al., 2018) and Tajikistan (Ding et al., 2002, Yang et al., 2020a), the Chinese Loess Plateau (Guo et al., 2002; Ding et al., 2005; Zan et al., 2018), and the fluviolacustrine sequences of the Gobi Desert (Sun and Liu, 2006; Chang et al., 2014) from the Late Pliocene. Except for these loess aeolian and fluviolacustrine deposits, uniform and fine lacustrine detritus convey more paleoclimatic information because the lithofacies are highly correlated with climatic change (Zhang et al., 2012b; Tan et al., 2020; Yang et al., 2020b); however, attaining complete and continuous Quaternary lacustrine sequences from the Tibetan Plateau has been a considerable challenge owing to poor exposure of the outcrop sections.

The rhombus-shaped Qaidam Basin, the largest intermontane basin on the NE Tibetan Plateau, is located in the transitional zone between the modern westerlies and the East Asian monsoon (Fig. 1). The westerly dominated climate controls the modern ecological environment of the western part of the basin, whereas the East Asian summer monsoon extends only to its southeastern section (Yang et al., 2020b). The basin has thick and continuous

*Corresponding author: Weilin Zhang, Email: zhangwl@itpcas.ac.cn

Cite this article: Zhang W, Li T, Fang X, Zhang T, Yan M, Zan J, Yang Y, Khatri DB (2021). Chronological and rock magnetic constraints on the transition of the Quaternary paleoclimate in the western Qaidam Basin, NE Tibetan Plateau. *Quaternary Research* **104**, 170–181. https://doi.org/10.1017/qua.2021.15

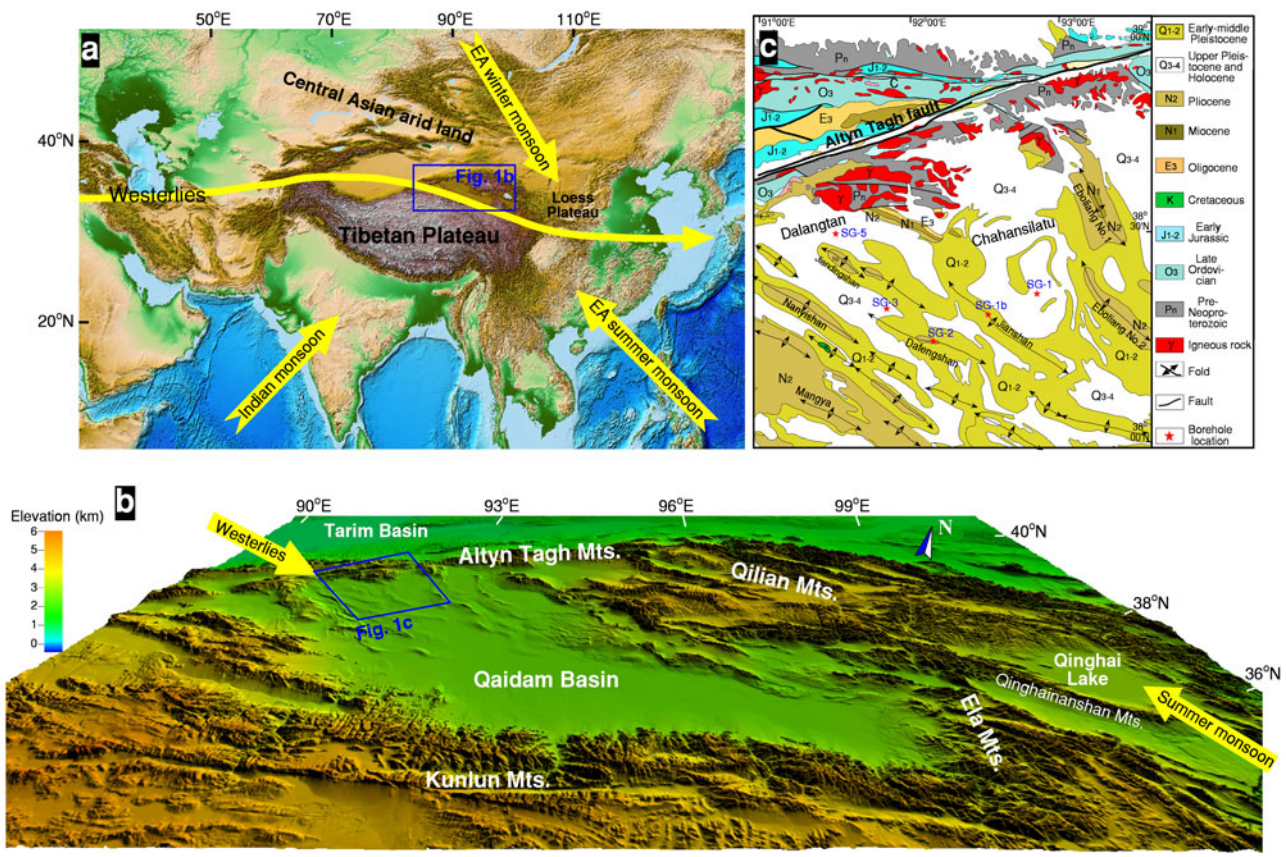

Figure 1. (color online) Digital elevation model and map of the Asian interior and its surrounding area showing the location of the Qaidam Basin and the influence of the westerlies and Asian monsoon (a), the Qaidam Basin and the surrounding mountains (b), and the study area and boreholes in the western Qaidam Basin (c).

sediments from the Eocene that record the interactions of tectonic uplift, Asian interior aridification, and global change (Huang et al., 1996; Xia et al., 2001; Wang and Burchfiel, 2004; Zhang et al., 2014; Fang et al., 2019).

To better understand the Quaternary climatic changes in the Asian interior, multiple boreholes, named SG-1, SG-1b, SG-2, and SG-3, have been extracted from the western Qaidam Basin since 2008 by a Sino-German research team in a joint scientific drilling framework. Numerous high-resolution paleoclimatic records, such as lithological transitions, grain size, geochemical proxies, and pollen spectra, have been successfully reported from the cores of these deep boreholes. Precise dating of magnetostratigraphic ages for the sediments from these boreholes is crucial for our understanding of Asian interior aridification, global cooling, and tectonic uplift of the NE Tibetan Plateau. In addition, research into the process and mechanism of long-term changes in rock magnetism has remained sparse in the fluvial and lacustrine deposits, hampering our knowledge of the paleoclimatic evolution in the Qaidam Basin (Zhang et al., 2012b; Tan et al., 2020). Here, we present the magnetostratigraphic results of the SG-5 borehole core to provide accurate age constraints on the stratigraphic framework. We use rock magnetic records to reconstruct the evolution of the Quaternary paleoclimate in central Asia.

GEOLOGICAL SETTING

The Qaidam Basin, with an average elevation of ~2800 m, is in the eastern section of the arid Asian interior. It is bordered by the Qilian Mountains to the north, the Kunlun Mountains to the south, the Altyn Tagh Mountains to the west, and the Ela Mountains to the east, with average elevations of ~4000–5000 m asl (Fig. 1a). The eastern Qaidam Basin, with a mean annual precipitation of 100–200 mm, contains widely distributed salt lakes and marshes. The western Qaidam Basin is extremely dry, with a mean annual precipitation of <20 mm, and is dominated by modern desert with gravel, sand deserts, and Yardang landforms. The whole basin has a mean annual temperature of 2–4°C, and the annual mean amount of evaporation reaches 3298 mm (Wang et al., 2012).

The Qaidam Basin has accumulated thick and continuous alluvial, fluviolacustrine, and lacustrine sediments since the Eocene. During its formation, the depocenter was located in its western part (Xia et al., 2001; Wang et al., 2006; Yin et al., 2008). With later tectonic uplift of the Kunlun and Altyn Tagh Mountains around the margins of the western basin, this part was subjected to strong tectonic compression and crustal shortening, causing multiple eastward shift steps of the depocenter and resulting in large variations in sediment thickness at different locations (Xia et al., 2001; Wang et al., 2006; Zhou et al., 2006; Yin et al., 2008). Since the Pliocene, the formerly uniform larger depocenter has broken and separated into several subdepressions (sub-basins), and closed paleolakes have formed (Yang et al., 2020b). These sub-basins have primarily deposited evaporites from the Late Pliocene (Shen et al. 1993; Cai et al., 2012; Wang et al., 2012). During the late Quaternary, the main depocenter of the basin shifted to the east (Gu et al., 1990; Huang et al., 1996;

https://doi.org/10.1017/qua.2021.15 Published online by Cambridge University Press

Xia et al., 2001; Wang et al., 2006). Meanwhile, the basin climate became drier, saline lake areas shrank, and the surface of the western basin became a playa with salt crusts (Wang et al., 2012).

The 6000-m-thick continuous sequence of Cenozoic sediments in the western Qaidam Basin was derived from the detritus of the surrounding mountains (Xia et al., 2001; Yin et al., 2002; Liu et al., 2009) and records paleoclimatic evolution in the Asian interior and the basin's deformation history associated with major tectonic upliftin the NE Tibetan Plateau (Yin et al., 2002; Wang and Burchfiel, 2004; Wang et al., 2012; Zhang et al., 2013, 2020). While thick layers of sandstone and conglomerate have characterized the margins of the western Qaidam Basin since the Late Pliocene, the thick and fine mudstone, marl, and evaporite deposited in the basin interior (Shen et al., 1993; Wang et al., 2012; Zhang et al., 2012a) could preserve significant climate information on Asian interior aridification and even on global cooling. Fine-grained sedimentary sequences were thus obtained from four boreholes drilled in the western Qaidam Basin. The sediments were magnetostratigraphically dated to ~2.77–0.1 Ma (SG-1 core with a depth of 938 m), 7.3–1.6 Ma (SG-1b core with a depth of 732 m), 3.7–3.2 Ma (SG-2 core with a depth of 151 m), and 3.06–0.1 Ma (SG-3 core with a depth of 600 m) (Fig. 1c; Cai et al., 2012; Zhang et al., 2012b, 2014, 2020). In thisarticle, the rock magnetic records are used to understand paleoclimatic changes in central Asia during the Quaternary, based on the accurate magnetostratigraphic ages of the SG-5 borehole core in the western Qaidam Basin.

MATERIALS AND METHODS

The SG-5 borehole (38°35.587′N, 91°28.234′E) was drilled on a flat playa in the Dalangtan salt lake in the western Qaidam Basin (Fig. 1). The core reached a depth of 590 m, with an average sedimentary recovery rate of ~90%. Its sedimentary sequence was dominated by gray clay silt, dark gray clay, calcareous mudstone, and gray-white halite, indicating a shallow-water lacustrine or fluvial environment throughout. The upper part of the core (0–225 m) is mainly composed of distinct thick gray-white halite and gray clay with a small amount of mirabilite and gypsum, which is an indicative of a shallow salt lake. The middle part (225–452 m) is dominated by gray or dark gray clay, clay silt, and calcareous mudstone interbedded with thin gray-white halite, indicating a transitional environment between shallow brackish lake and salt lake. The lower part of the core (452–590 m) is mainly characterized by coarse brownish yellow sandstone, with conglomerates in the bottom, gray clay and mudstone in the middle, and gray siltstone and fine sandstone in the upper sections; these can be interpreted as braided river and overbank deposits.

The degree of cementation of the sandstone and conglomerates in the bottom of the SG-5 borehole is weak; therefore, all samples were taken from the fine sediments at depths ranging from 0 to 511 m. A total of 1030 cubic (2 × 2 × 2 cm) specimens at ~50-cm intervals and 1373 specimens at ~30-cm intervals were taken for the magnetostratigraphic study and the rock magnetic analysis, respectively. All the magnetostratigraphic samples were subjected to stepwise alternating field demagnetization (AFD) at fields up to 140 mT with 4- or 20-mT increments. All remanence measurements were made using a 2 G Enterprises Model 755 cryogenic magnetometer installed in a field free space (<150 nT) at the Institute of Tibetan Plateau Research, Chinese Academy of Sciences. The rock magnetic specimens were measured using a Bartington MS2 susceptometer at frequencies of 470 Hz and 4700 Hz. The values of mass-specific frequency-dependent magnetic susceptibility (χ_{fd}) and percentage frequency-dependent magnetic susceptibility (χ_{fd} %) were defined as $\chi_{fd} = \chi_{470Hz} - \chi_{4700Hz}$ and $\chi_{fd}\ \% = (\chi_{470Hz} - \chi_{4700Hz}) / \chi_{470Hz} \times 100\%$. The anhysteretic remanent magnetization (ARM) was measured using a 100-mT peak alternating field and a superimposed 0.05 mT direct current biasing field by a D-2000 alternating demagnetizer, and the susceptibility of ARM (χ_{ARM}) was calculated as ARM/0.05 mT. The saturation isothermal remanent magnetization (SIRM) was acquired with an IM-10-30 pulse magnetizer in a magnetic field of 1 T.

The temperature-dependent magnetic susceptibilities (χ-T) of the typical samples, each of which had a mass of ~0.2 g, were measured under an argon atmosphere to avoid oxidation during heating from room temperature to ~700°C and then cooled to room temperature using a MFK1-FA Kappabridge and a CS-4 high-temperature furnace (Agico Ltd., Brno, Czech Republic). Magnetic hysteresis parameters, including hysteresis loops and isothermal remanent magnetization (IRM) acquisition curves, were measured on a Lakeshore vibrating sample magnetometer 8600 with a maximum applied field approaching 1 T. The paramagnetic susceptibilities of the hysteresis loops were removed by slope correction between 800 and 1000 mT. Several magnetic parameters were determined, including the saturation magnetization (Ms), saturation remanent magnetization, and coercivity (Bc).

RESULTS

χ-T curves, hysteresis loop, and IRM acquisition curves

All χ-T curves generally exhibited higher susceptibility to cooling than heating (Fig. 2), possibly indicating that stronger magnetic minerals, such as magnetite, which formed during cooling oxidize from iron-containing paramagnetic minerals existing in the sediments. For the samples with high and low magnetic susceptibility (χ) values, almost all heating curves show a peak value in susceptibility between 300 and 500°C (Fig. 2).This can be interpreted as the formation of ferrimagnetic minerals, such as magnetite, by the oxidization of iron sulfides during heating (Roberts et al., 1995). Obvious losses of susceptibility occurred at ~580°C, and minimum values above 690°C were observed, implying that the samples carry magnetite and hematite.

After paramagnetic slope correction, all hysteresis loops were almost closed before reaching 300 mT, and the Bc values were lower than 40 mT, indicating the dominance of soft ferrimagnetic minerals. In addition, the Ms of the samples with a low χ value are less than 6.5×10^{-3} Am^2/kg (Fig. 3a), considerably lower than that of the samples with a high χ value (Ms $>16.0 \times 10^{-3}$ Am^2/kg) (Fig. 3b), implying that the concentration of ferrimagnetic minerals in the latter is higher than in the former.

The IRM acquisition curves show rapid increases below 200 mT, and most samples acquired at least 90% of SIRM at ~300 mT (Fig. 4), further demonstrating that magnetic minerals for the SG-5 borehole core were dominated by low-coercivity minerals. Nevertheless, IRMs in individual samples still have no complete saturation value when the applied field gradually increased to 1 T (Fig. 4), reflecting the presence of hard magnetic minerals. The maximum of SIRM is $<1.\ 5 \times 10^{-3}$ Am^2/kg for the samples with a low χ value and $>2.5 \times 10^{-3}$ Am^2/kg for those with a high χ value (Fig. 4), also indicating that a high concentration of ferrimagnetic minerals exists in samples with a high χ value, which is consistent with the results of the hysteresis loops.

https://doi.org/10.1017/qua.2021.15 Published online by Cambridge University Press

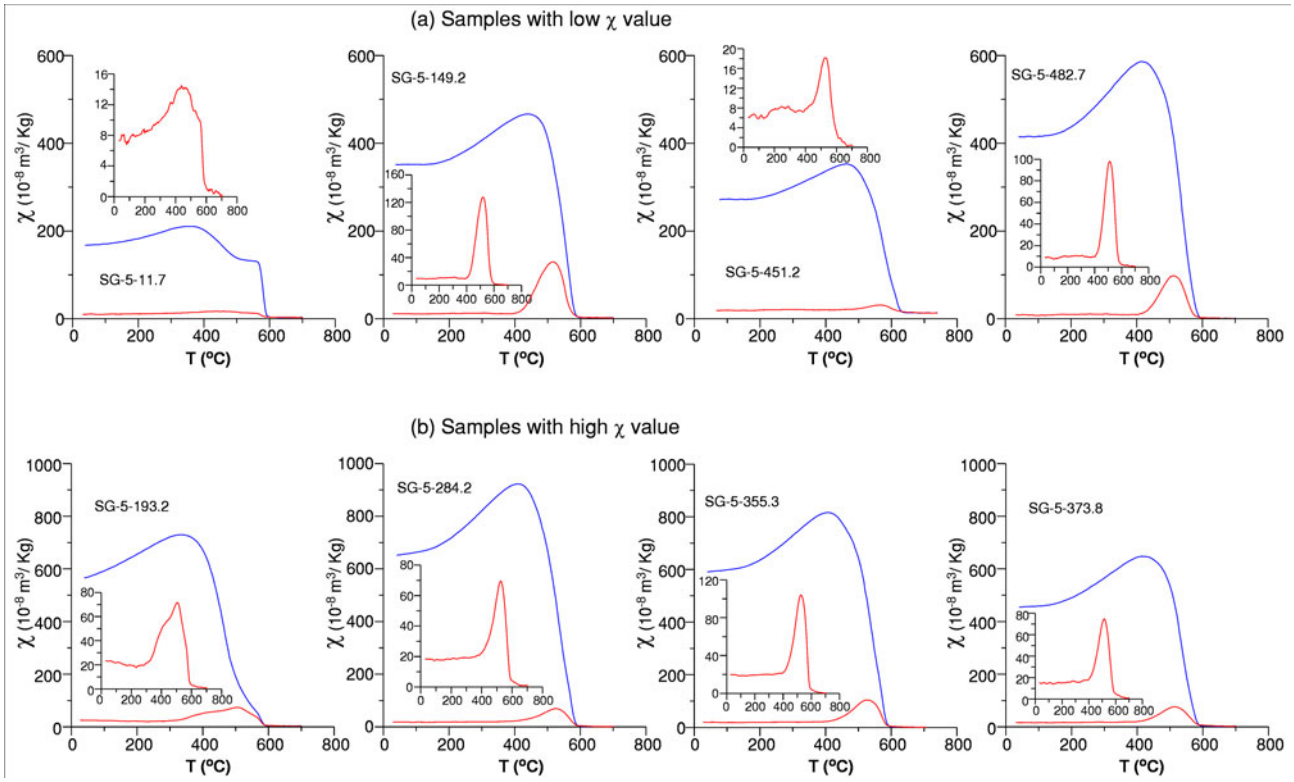

Figure 2. High-temperature magnetic susceptibility (χ-T) curves of typical samples from the borehole SG-5 core. (a) Typical data from the samples with a low magnetic susceptibility (χ) value. (b) Typical data from the samples with a high χ value. Red and blue lines represent heating and cooling χ-T curves, respectively; the inset small plots show the amplified scales for heating χ-T curves. (For interpretation of the references to color in this figure legend, the reader is referred to the web version of this article.)

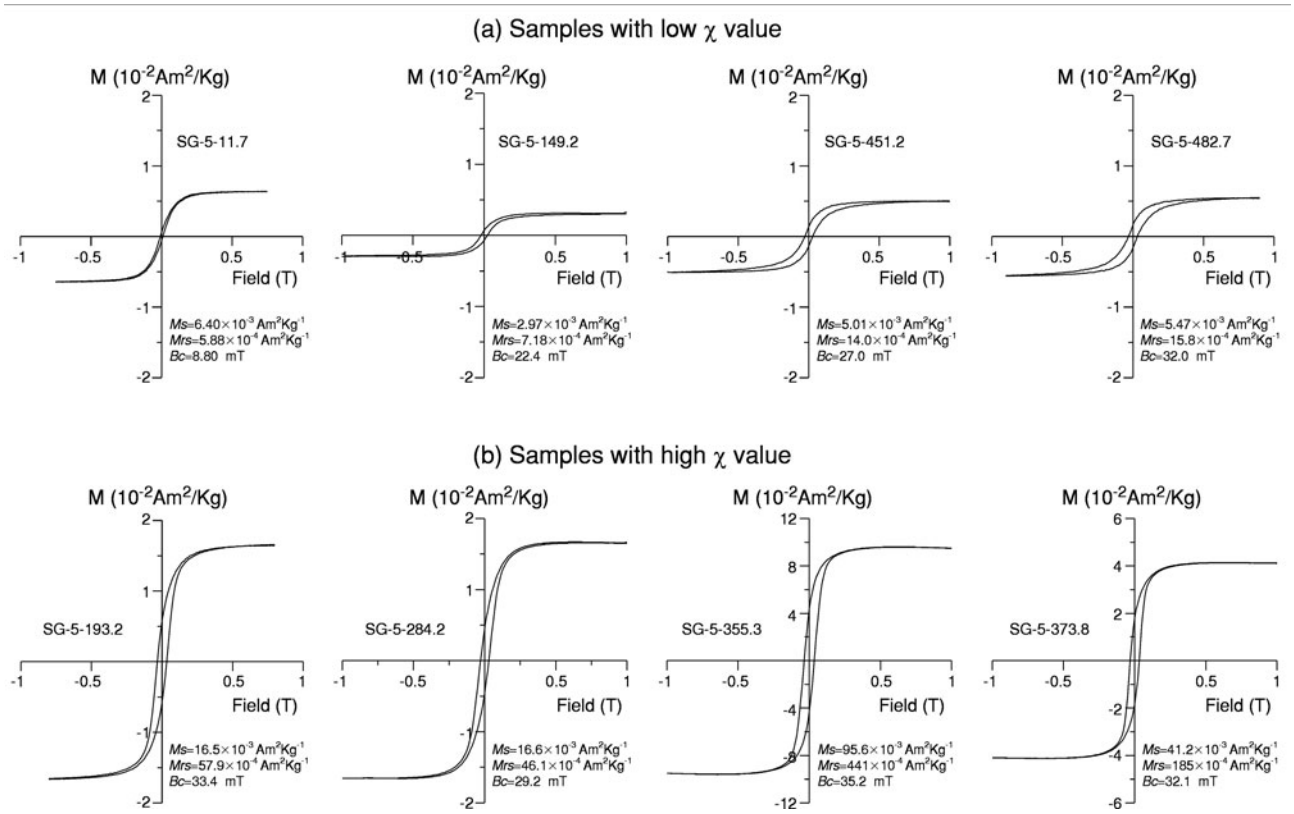

Figure 3. Magnetic hysteresis loops (after slope correction) from the samples with a low χ value (a) and a high χ value (b) from the SG-5 borehole core.

https://doi.org/10.1017/qua.2021.15 Published online by Cambridge University Press

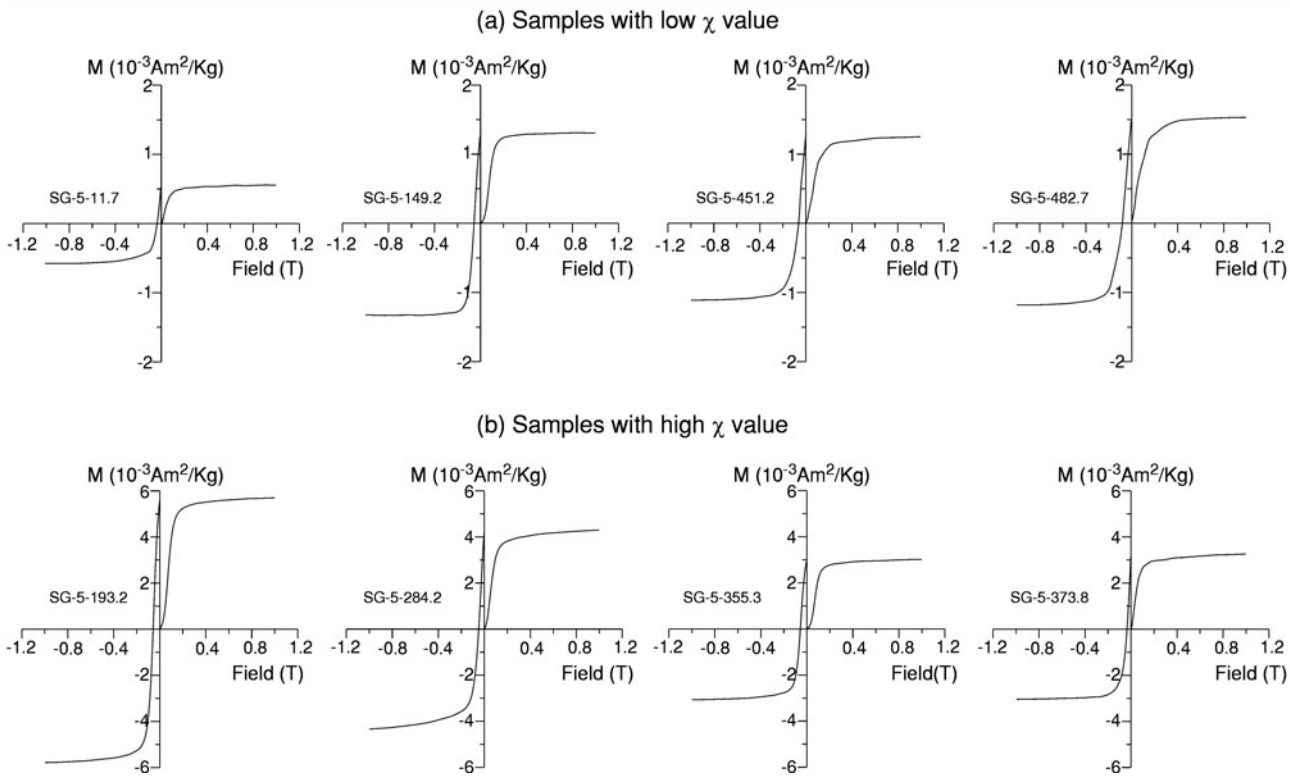

Figure 4. Isothermal remanent magnetization acquisition curves from samples with a low χ value (a) and a high χ value (b) for the SG-5 borehole core.

Alternating field demagnetization characteristics and magnetostratigraphy

Based on the aforementioned results on the soft magnetic mineral for the dominant contributions of the SG-5 borehole core, which is similar to rock magnetic results from the SG-1, SG-1b, and SG-3 borehole cores (Zhang et al., 2012a, 2012b, 2020; Tan et al., 2020), AFD was applied to analyze the characteristic remanent magnetization (ChRM) component. The AFD plots show the soft component was a relatively softer magnetic mineral or a viscous overprint demagnetized before 20 mT, and the ChRMs were clearly isolated and pointed directly toward the origin in the Zijderveld diagram after 20 mT (Fig. 5). Relatively higher ChRM values imply that the small residual remanence after 140 mT resides in the highest coercive hematite. These observations, in agreement with the χ-T curves, IRM, and magnetic hysteresis loops (Figs. 2–4), confirm that the major contributors of ChRMs are magnetite, followed by small amounts of hematite.

The ChRM directions were calculated by at least four consecutive demagnetization steps over 30 mT. Directions with a maximum angular deviation of >15° were rejected. A total of 797 samples (out of 1030 measured samples) had stable ChRM directions; the declinations were insignificant, with no control on the core azimuth during drilling, and only the inclinations were further used to interpret magnetostratigraphic ages. At least two consecutive samples with the same polarity were used to define a polarity interval as an excursion or event. A total of 34 normal (N1–N17) and reversed (R1–R17) polarity zones were identified in the SG-5 borehole (Fig. 6).

χ, χ_{fd}, χ_{fd} %, χ_{ARM}, and SIRM

The values of mass-specific χ in the SG-5 borehole core vary from 0.86×10^{-8} m^3/kg to 4.93×10^{-7} m^3/kg, with subtle increasing and decreasing trends at depths of ~220 m along the entire core (Fig. 6). Mudstone and siltstone layers intercalated with salt-bearing layers have much higher χ values than those of evaporite layers. The χ_{fd} and χ_{fd} % are generally low, with values of $<0.5 \times 10^{-8}$ m^3/kg and <5%, with no large variations over the entire core (Fig. 6), indicating that the contribution of ultrafine ferrimagnetic minerals to χ variations can be neglected.

SIRM is an effective index to estimate the total concentration of magnetic minerals with grain sizes above the threshold of superparamagnetic and single-domain (SD) grains (Thompson and Oldfield, 1986; Evans and Heller, 2003), and χ_{ARM} is usually sensitive to SD grains (Maher, 1988; Evans and Heller, 2003). The overall trends of SIRM and χ_{ARM} in the SG-5 borehole core, with their values varying from $\sim 0.18–159 \times 10^{-4}$ Am^2/kg and $\sim 0.05–20.8 \times 10^{-7}$ m^3/kg, respectively, show similar variations of χ across the entire core (Fig. 6), indicating that the concentrations of magnetic minerals with SD grains result in variations of χ in the sediments of the paleolake in the western Qaidam Basin; this was similar to the previous rock magnetic analyses from the SG-1 and SG-3 boreholes (Zhang et al., 2012a; Tan et al., 2020).

DISCUSSION

Magnetostratigraphic age constraint on the strata since the Late Pliocene

The SG-5 borehole site is located in the western part of the Dalangtan depression, which has a flat surface covered by a salt crust. Its topmost sediments are presumed to be of subrecent age. Previous work demonstrated that surface age was dated at ~0.1 Ma by the magnetostratigraphy of the depression and its adjacent Chahansilatu-deposited zones with the desiccated playa

https://doi.org/10.1017/qua.2021.15 Published online by Cambridge University Press

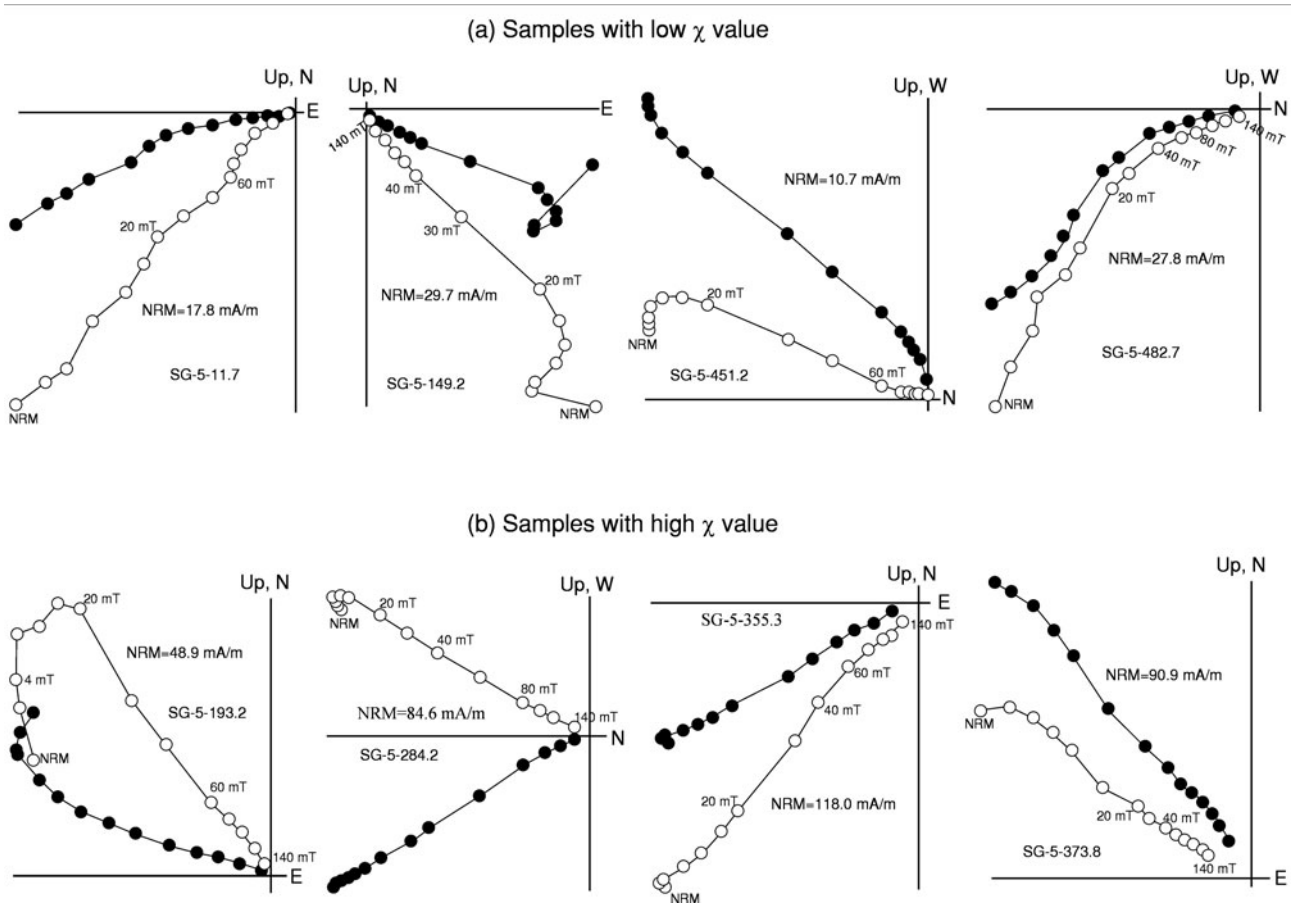

Figure 5. Results of alternating field demagnetization for samples with a low χ value (a) and a high χ value (b) from the SG-5 borehole core. Open and closed circles represent vertical and horizontal projections, respectively.

(Shi et al., 2010; Cai et al., 2012; Zhang et al., 2012b). OSL and U-Th dating also constrained the playa salt crust of the western Qaidam Basin to be ~0.1 Ma (Han et al., 2013). Based on the top salt crust, the observed polarity zones (N1–N17 and R1–R17) from the SG-5 borehole core correlate well with the chrons C1n–C2An.1r of the Geomagnetic Polarity Time Scale (GPTS) 2012 (Fig. 6; Gradstein et al., 2012). The top normal polarity zones N1–N6 most likely correspond to the Brunhes normal polarity epoch; the other short reverse polarity zones R1–R5 can be interpreted as CR0, Portuguese margin, Delta, Levantine, Emperor, and Big Lost or Delta events, respectively (Fig. 6; Champion et al., 1988; Langereis et al., 1997; Lund et al., 2006; Laj and Channell, 2007; Thouveny et al., 2008; Gradstein et al., 2012). The reverse polarity zones R6–R16 can be interpreted as the Matuyama polarity epoch. The normal polarity zones N7–N10, N13, and N14 within the Matuyama epoch can be readily correlated with Jaramillo, Cobb Mountain, Bjorn, Gardar, Olduvai, and Reunion normal subchrons, respectively. The lowest polarity zones are characterized by one long normal and one short reverse polarity zone, N17 and R17, which likely record the middle–upper part of the Gauss normal polarity epoch, such as C2An.1n and C2An.1r. Assuming these correlations, the SG-5 borehole core is determined to have an age ranging from 0.1 to 3.0 Ma, with the Brunhes/Matuyama and Matuyama/Gauss boundaries located at depths of 94.5 and 447.0 m, respectively. The observed short normal polarity intervals N6, N11, N14, and N15 remain less secure in our correlation, but this should not grossly affect the above correlations with the GPTS 2012.

Paleomagnetic investigations of multiple borehole cores from the adjacent area also show a similar magnetostratigraphic age framework (Fig. 7a–e; Cai et al., 2012; Zhang et al., 2012b, 2014, 2020). Based on the proposed magnetostratigraphic age interpretations of the SG-1, SG-1b, and SG-2 borehole strata, the youngest ages of the centers of the Dafengshan and Jianshan anticlines are 1.6 and 3.2 Ma (Fig. 7f), indicating unroofing since the Late Pliocene strata took place at ~3.2 and ~1.6 Ma (Zhang et al., 2020). The composite lithology analysis shows that the SG-1 and SG-3 borehole cores from the Dalangtan and Chahansilatu depressions were characterized by gray mudstone gypsum and halite before 1.2 Ma (Fig. 7c, e, f), representing a saline paleolake environment. The lithofacies analysis of the SG-1b and SG-2 borehole cores imply that the Dafengshan and Jianshan anticline hinges were shallow paleolake depositional environments before 1.2 Ma, characterized by clay, mudstone, and marl intercalated with scattered gypsum and thin salt layers (Fig. 7a, f).

It is generally considered that the salt beds were synchronously deposited in the central part of the western Qaidam Basin, but this is not the case from the foregoing magnetostratigraphic strata. The most reasonable explanation for this case is that offlap growth strata became progressively younger from the southwest to northeast in the center of the western basin owing to a strong fault

https://doi.org/10.1017/qua.2021.15 Published online by Cambridge University Press

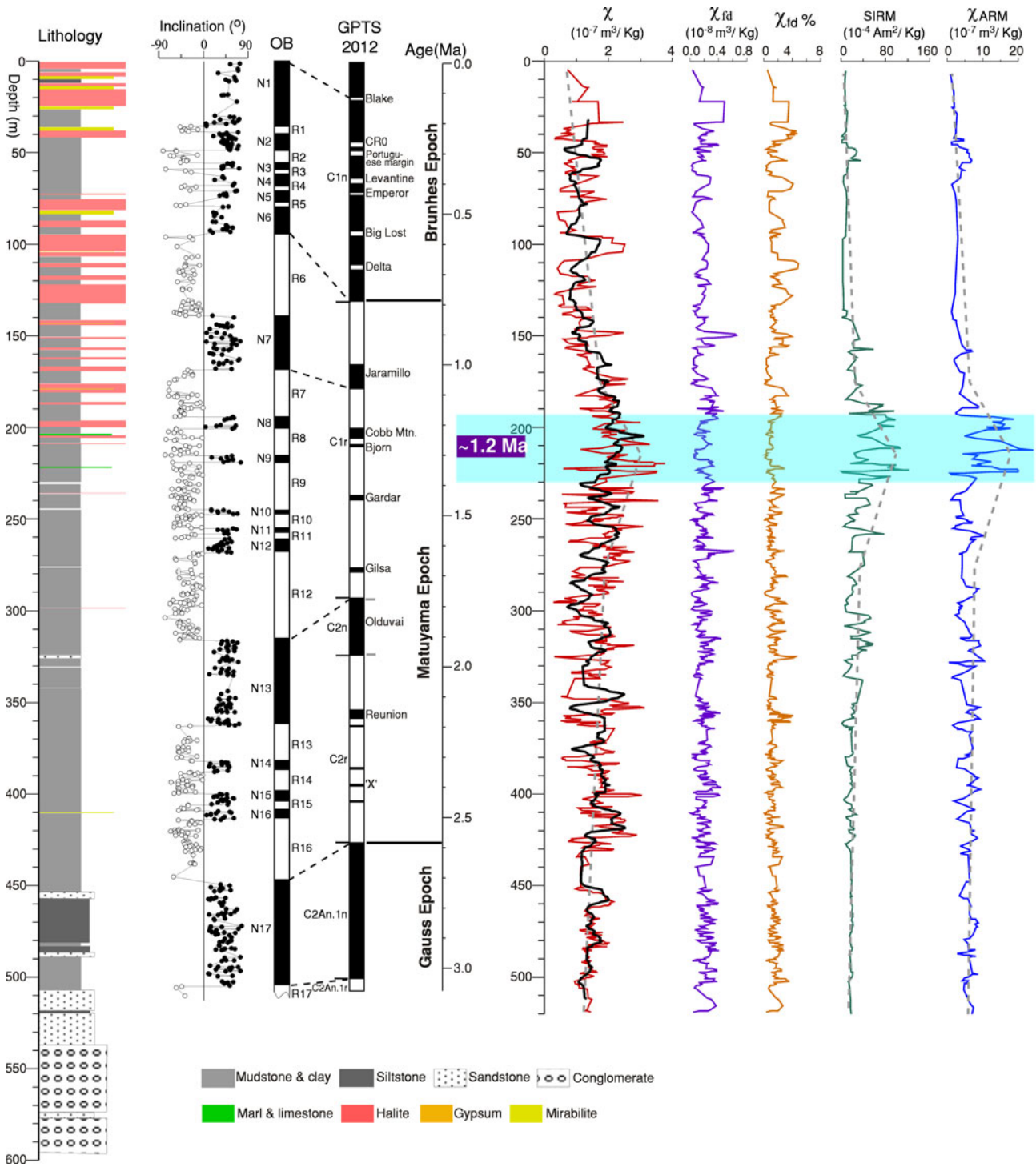

Figure 6. (color online) Lithology, magnetostratigraphy (black/white bars indicate normal/reversed polarity), and records of χ, mass-specific frequency-dependent magnetic susceptibility (χ_{fd}), percentage frequency-dependent magnetic susceptibility (χ_{fd} %), saturation isothermal remanent magnetization (SIRM), and susceptibility of mass-specific anhysteretic remanent magnetization (χARM) for the SG-5 borehole core. Note that the bolded black line in the χ record represents the curve of an 11-point running average; the dashed gray lines represent the general change trend of rock magnetic records; GPTS = Geomagnetic Polarity Time Scale. Note that all the data for this figure can be found in the supplementary material.

basinward propagation (Zhang et al., 2014, 2020). This resulted in the anticline hinge becoming the lakeshore area and allowing the inflow of fresh water (Fig. 7f), confirmed by the conglomerates deposited at the SG-2 and SG-5 boreholes by a braided river channel (Fig. 7a, b). The thickness of the salt layers increased gradually after 1.2 Ma in the western Qaidam Basin, regardless of whether it was the hinge or limb of the anticline (Fig. 7b, c, e). The pattern and migration of paleorivers could have highly influenced the salt formation in the depressions (Yuan et al., 1983; Duan and Hu, 2001; Wang et al., 2006), whereas the persistent inflow of snow melt from the Kunlun, Altyn Tagh, and Qilian Mountains have not suppressed the formation of salt layers in the Quaternary

https://doi.org/10.1017/qua.2021.15 Published online by Cambridge University Press

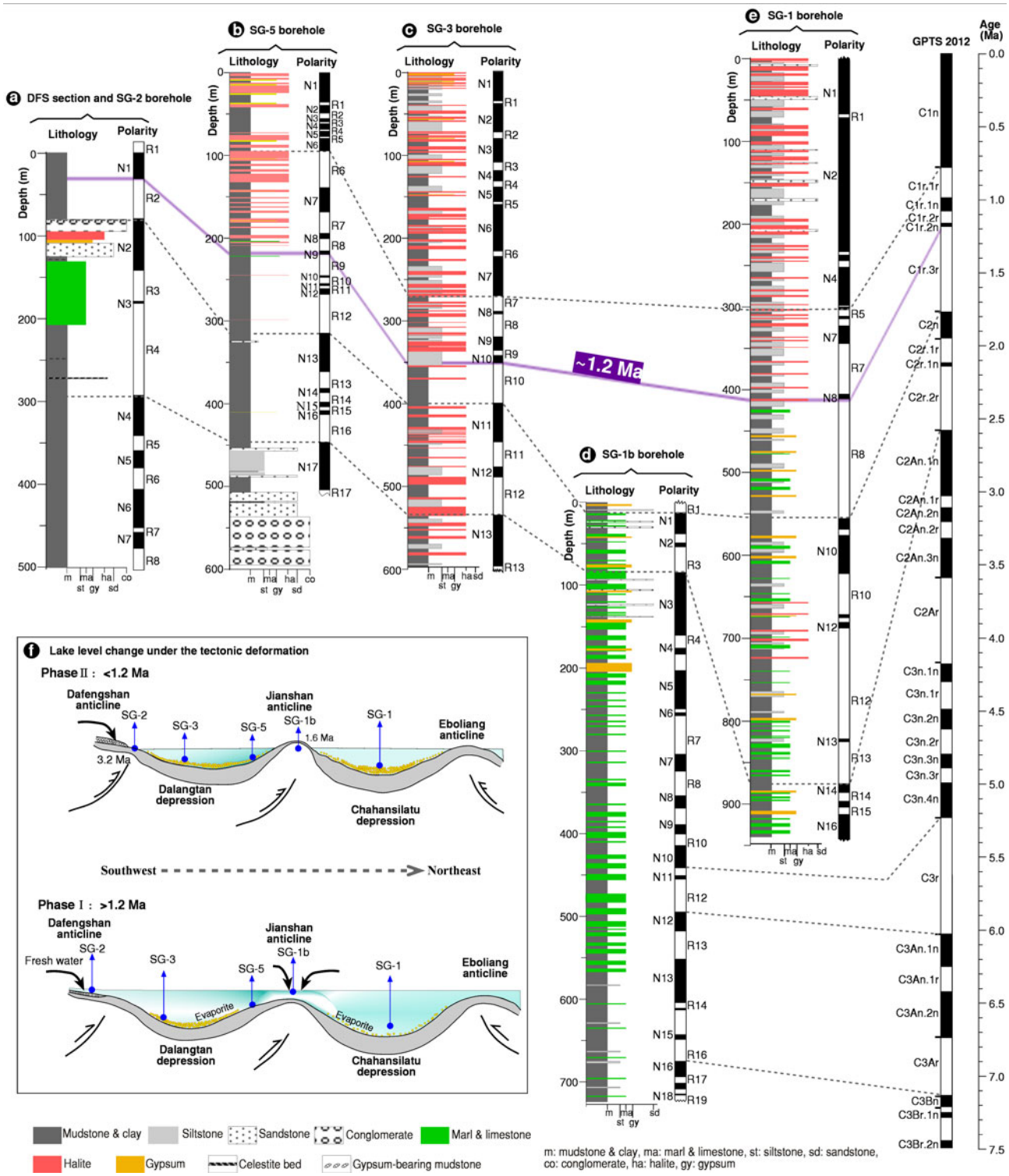

Figure 7. (color online) Correlations of lithologies and magnetostratigraphies of the borehole cores, with the GPTS from the borehole cores in the western Qaidam Basin (A–E) and dynamic models for the change of the lithology and shifts of the sedimentary center in the paleolake of the western Qaidam Basin before and after 1.2 Ma (F).

depressions. Thus, the comparisons of the magnetostratigraphic ages from the different locations of the western Qaidam Basin can provide more precise time constraints for the climatic and tectonic strata.

The magnetostratigraphic ages on the top of the SG-1, SG-3, and SG-5 borehole cores demonstrate that the termination of evaporite deposition occurred at ~0.1 Ma in the western Qaidam Basin (Fig. 8; Cai et al., 2012; Zhang et al., 2012b); this is also supported by the OSL and U-Th dating of the playa salt crust (Han et al., 2013). Owing to strong rapid uplift since the mid-Pleistocene, syntectonic growth strata became more prominent. The basin depocenter shifted eastward and ultimately

https://doi.org/10.1017/qua.2021.15 Published online by Cambridge University Press

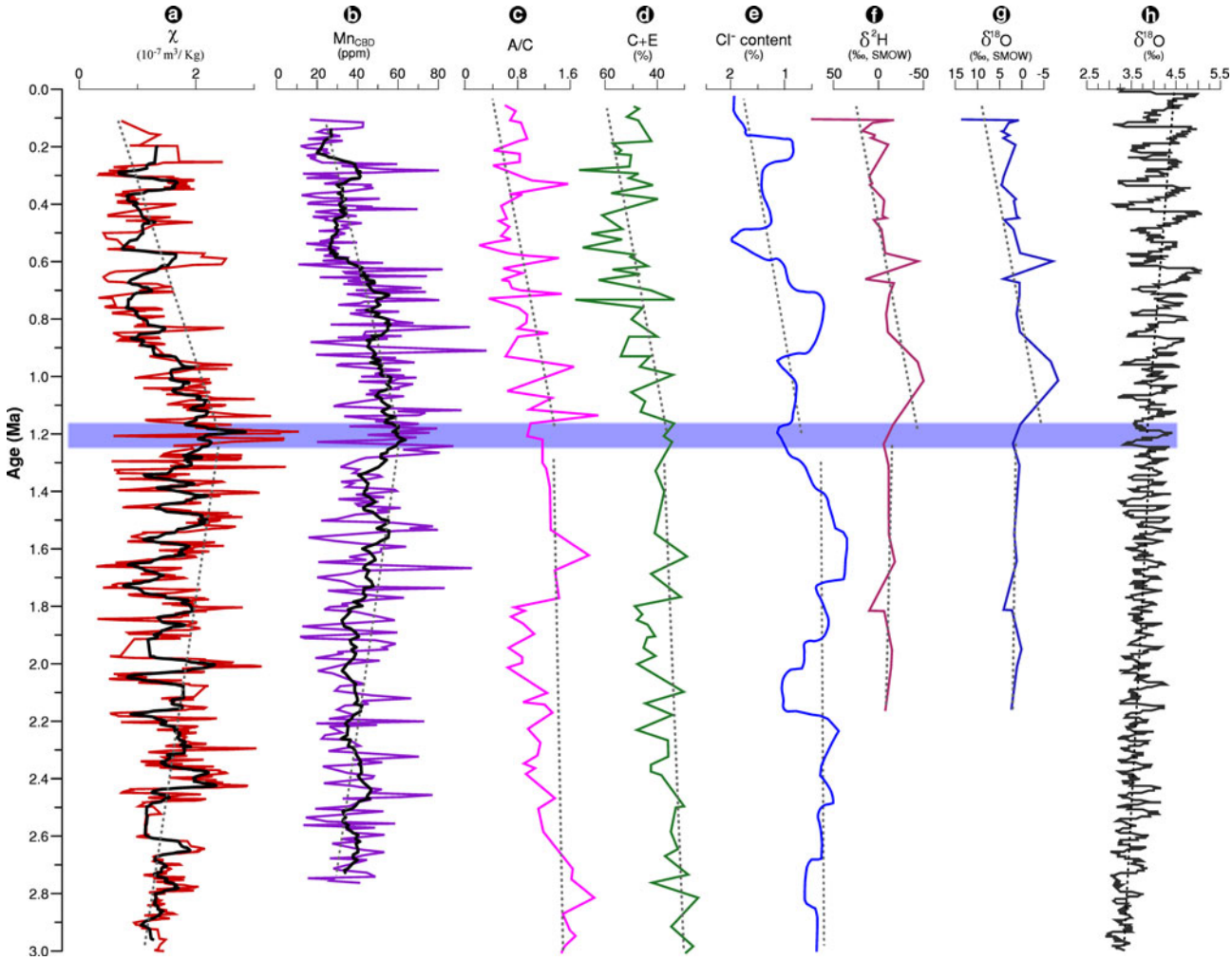

Figure 8. (color online) Comparisons of climatic and environmental records in the western Qaidam Basin with global climatic records since 3.0 Ma. (a) χ of the borehole SG-5 core, including an 11-point running average line. (b) Manganese (Mn) concentrations from the citrate-bicarbonate-dithionite extraction (Mn_{CBD}), including an 11-point running average line (Yang et al., 2013). (c, d) *Artemisia*/Chenopodiaceae (A/C) and Chenopodiaceae and Ephedraceae (C+E) xerophytic taxa () records (Cai et al., 2012). (e) Chloride (Cl-) content representing paleosalinity evolution of the western Qaidam Basin (Guo et al., 2018). (f, g) $\delta^{18}O$ and $\delta^{2}H$ values of fluid inclusions in gypsum crystals (Li et al., 2017). (h) Global marine sediment $\delta^{18}O$ record from LR04 (Lisiecki and Raymo, 2005). The dashed gray line represents the change trend of each record; SMOW = Standard Mean Ocean Water.

withdrew from the Dalangtan and Chahansilatu depressions at 0.1 Ma (Zhang et al., 2014), leading to the formation of the largest saline lake in the Qarhan depression in the eastern Qaidam Basin. After 0.1 Ma, most of the western basin had become a denudation area and suffered erosion by the strong westerlies and regional winds, finally forming the present Yardang landform or salt crust (Han et al., 2013; Zhang et al., 2020). The magnetostratigraphic age constraints on the lithofacies demonstrate that, while tectonic uplifts contributed to the shifts in the depocenter of the basin, they did not transform its climate pattern (Zhang et al., 2014; Lu et al., 2015; Yang et al., 2020b). Asian interior aridification and global cooling were the significant influencing factors of the basin's environment.

Transition of the Quaternary paleoclimate in the western Qaidam Basin

The lacustrine sediments from the western Qaidam Basin are closely related to the evolution of the westerlies system associated with global change. The χ of the fine sediments has been regarded as a proxy index of the intensity of the westerly jets and global cooling (Zhang et al., 2012a; Tan et al., 2020; Yang et al., 2020b) and/or the paleoclimatic changes of the Qaidam Basin driven by the closure of the Indonesian seaway (Su et al., 2019). Based on the magnetostratigraphic age constraints on the multiple borehole cores, our observed χ gradually increased between 3.0 and 1.2 Ma, attained its peak at 1.2 Ma, and subsequently showed a gradual decline (Fig. 8a). Since χ is a significant climate signal, we infer that one climate transition event occurred in the western Qaidam Basin at 1.2 Ma.

From the rock magnetic results presented above, the variation of χ in the SG-5 borehole core appears to be caused by the relative concentration of magnetic minerals in the clastic deposits, which is similar to the inferences from the SG-1 borehole cores. From the overall changing trend of χ, the SG-5 boreholes exhibited the same long-term decrease in the anticline limb of the western Qaidam Basin as the SG-1 and SG-3 boreholes (Zhang et al., 2012a; Tan et al., 2020), while the anticline hinge as the SG-5

https://doi.org/10.1017/qua.2021.15 Published online by Cambridge University Press

borehole showed a trend of first increasing and then decreasing values of χ, with the transitional boundary at 1.2 Ma. The evaporite content from all these borehole cores also gradually increased after 1.2 Ma (Fig. 8b, c, e); therefore, the two original models on low-temperature oxidation or provenance change (Zhang et al., 2012a) should be reconsidered. Low-temperature oxidation can lead to the formation of hematite via preexisting magnetite or maghemite. The provenance alternations caused by the glacial-interglacial cycles during the Quaternary should transform the type of magnetic mineral or the size of magnetic grains, which is inconsistent with no more hematite in our SG-5 borehole and dominant SD grains in the SG-3 borehole (Tan et al., 2020). In addition, the pedogenesis model for magnetic properties is only present in the floodplain within the fluvio-lacustrine sediments (Ao et al., 2010) or in the loess-paleosol (Zan et al., 2018). Thus, this model is only one explanation for Asian interior aridification and global cooling for the χ variations in the western Qaidam Basin.

During the Pliocene to Quaternary, the climate turned toward dry and cold conditions (Cai et al., 2012; Wang et al., 2013; Han et al., 2014; Guo et al., 2018), which played an important role for salt formation in the Qaidam Basin. The salt deposits altered the relative content of the detritus and further diluted the concentration of magnetic minerals. Before 1.2 Ma, the dry, cold climate resulted in the gradual formation of thick evaporite layers and a decrease in the proportion of detrital material in the anticline limb of the western Qaidam Basin, as indicated by the decrease of χ values in the SG-1 borehole at the center of the Chahansilatu depression (Fig. 7f). In comparison with the anticline limb in the middle of the paleolake, the anticline hinge, which had high altitude and was the paleolakeshore, deposited massive detritus denuded by strong cryoclastic erosion during the dry, cold phase, and aeolian sediments were deposited by the westerly jet and supply of snowmelt fresh water, which made it very difficult to form evaporite beds and led to the gradual increase of χ values in the SG-5 borehole.

After 1.2 Ma, accompanied by a drier and colder climate in the Asian interior in the late Quaternary (Lü et al., 2001; Fang et al., 2002; Ding et al., 2005; Wu et al., 2007; Zan et al., 2010), the whole western Qaidam Basin began to turn into a large area of salt-lake deposits, including the limb and hinge of the anticline, and the paleolake began to dry (Fig. 7f). Meanwhile, a high concentration of evaporites here diluted the relative content of detritus, indicating a lower χ value after 1.2 Ma. This χ variation mechanism on Asian interior aridification and global cooling is reasonable for long-term changing trends of χ in different regions of the western Qaidam Basin. Though rapid tectonic uplifts amplified the glaciation and erosion of the surrounding mountains and adjusted the shifts of the basin depocenter, they were not enough to change the aridification environment of the whole basin. Thus, we suggest that at 1.2 Ma, the western Qaidam Basin experienced a significant climatic transition under Asian interior aridification and global cooling.

The mid-Pleistocene climate transition between 1.2 and 1.1 Ma brought the global climate system into the late Pleistocene ice ages (Ruddiman et al., 1989; Mudelsee and Schulz, 1997; Berger et al., 1999; Schmieder et al., 2000; Clark et al., 2006), and the Asian interior experienced further aridification (Fang et al., 1999; An et al., 2001; Han et al., 2012; Song et al., 2014). In the western Qaidam Basin, the manganese content analyzed by the citrate-bicarbonate-dithionite extraction showed a gradual increase before 1.2 Ma, with peak values at 1.2 Ma and a subsequent decreasing trend after 1.2 Ma (Fig. 8b; Yang et al., 2013, 2016), indicating paleolake redox changes and a drying climate. The ratios of *Artemisia*/Chenopodiaceae (Fig. 8c) and the value of xerophytic taxa from Chenopodiaceae and Ephedraceae (Fig. 8d) also exhibited a significant climate change at 1.2 Ma (Cai et al., 2012). The chloride content, a common lake-water paleosalinity index, exhibited abrupt increases at ~1.2 Ma, indicating the wide distribution of the playa in the western Qaidam Basin after 1.2 Ma due to global cooling and Asian interior aridification or the eastward shift of the basin depocenter under tectonic uplifts (Fig. 8e; Guo et al., 2018). The $\delta^{18}O$ and $\delta^{2}H$ values of fluid inclusions from primary gypsum crystals recording lake-water conditions indicated an important variation with a cold and dry event at 1.2 Ma (Fig. 8f, g; Li et al., 2017).

These findings on climate change at 1.2 Ma in the western Qaidam Basin are synchronous with long-term global cooling, with fluctuations at 1.2 Ma inferred from the deep-sea oxygen isotope record (Fig. 8h; Lisiecki and Raymo, 2005). In summary, χ and other climatic records suggest that the Quaternary climate of the western Qaidam Basin experienced an important transition at 1.2 Ma related to Asian interior aridification and global cooling.

CONCLUSIONS

Magnetic polarity stratigraphic analysis of the stratigraphic sequence from the SG-5 borehole yield estimated ages between 3.0 and 0.1 Ma. Based on magnetostratigraphic ages of multiple borehole cores, the initial salt beds in the limb of anticline are older than in the hinge of anticline in the western Qaidam Basin. The strata for the obvious alterations of evaporite content and χ values are constrained by the magnetostratigraphic age to 1.2 Ma. A comparison of magnetostratigraphic, χ, pollen, salt ion, and grain-size results from adjacent borehole cores demonstrate that the Quaternary climate of the western Qaidam Basin experienced a significant environmental transition at 1.2 Ma related to Asian interior aridification and global cooling.

Supplementary Material. To view supplementary material for this article, please visit https://doi.org/10.1017/qua.2021.15

Acknowledgments. We especially thank Zhao Yan, Sun Shurui, Tian Qian, Yang Rongsheng, Yang Yongpeng, Li Yuwen, and Lu Yin for the cutting and sorting of the cores from the SG-5 borehole. We are grateful to Editor Derek Booth, Reviewer John Dodson, and an anonymous reviewer for the constructive comments and improving the English.

Financial Support. This work was cosupported by the National Natural Science Foundation of China (grants 41672358, 41620104002, 41872098), the Second Tibetan Plateau Scientific Expedition and Research (grant 2019QZKK0707), the Strategic Priority Research Program of the Chinese Academy of Sciences (grant XDA20070201), the National Basic Research Program of China (grant 2017YFC0602803), and the German Ministry for Education and Research BMBF within WTZ Zentralasien (grant 03G0805A).

REFERENCES

An, Z., Kutzbach, J.E., Prell, W.L., Porter, S.C., 2001. Evolution of Asian monsoons and phased uplift of the Himalaya–Tibetan Plateau since Late Miocene times. *Nature* **411**, 62–66.

Ao, H., Deng, C., Dekkers, M.J., Liu, Q., 2010. Magnetic mineral dissolution in Pleistocene fluvio-lacustrine sediments, Nihewan Basin (North China). *Earth and Planetary Science Letters* **292**, 191–200.

Berger, A., Li, X.S., Loutre, M.F., 1999. Modelling Northern Hemisphere ice volume over the last 3 Ma. *Quaternary Science Reviews* **18**, 1–11.

Bosboom, R.E., Abels, H.A., Hoorn, G., Van den berg, B.C.J., Guo, Z., Dupont-Nivet, G., 2014. Aridification in continental Asia after the Middle Eocene Climatic Optimum (MECO). *Earth and Planetary Science Letters* **389**, 34–42.

Bosboom, R.E., Dupont-Nivet, G., Houben, A.J.P., Brinkhuis, H., Villa, G., Mandic, O., Stoica, M., *et al.*, 2011. Late Eocene sea retreat from the Tarim Basin (West China) and concomitant Asian paleoenvironmental change. *Paleogeography, Paleoclimatology, Paleoecology* **299**, 385–398.

Cai, M., Fang, X., Wu, F., Miao, Y., Appel, E., 2012. Pliocene–Pleistocene stepwise drying of central Asia: evidence from paleomagnetism and sporopollen record of the deep borehole SG-3 in the western Qaidam Basin, NE Tibetan Plateau. *Global and Planetary Change* **94–95**, 72–81.

Champion, D.E, Lanphere, M.A., Kuntz, M.A., 1988. Evidence for a new geomagnetic reversal from lava flows in Idaho: discussion of short polarity reversals in the Brunhes and late Matuyama polarity chrons. *Journal of Geophysical Research* **93**, 11667–11680.

Chang, H., An, Z., Liu, W., Ao, H., Qiang, X., Song, Y., Lai, Z., 2014. Quaternary structural partitioning within the rigid Tarim plate inferred from magnetostratigraphy and sedimentation rate in the eastern Tarim Basin in China. *Quaternary Research* **81**, 424–432.

Clark, P.U., Archer, D., Pollard, D., Blum, J.D., Rial, J.A., Brovkin, V., Mix, A.C., Pisias, N.G., Roy, M., 2006. The middle Pleistocene transition: characteristics, mechanisms, and implications for long-term changes in atmospheric pCO_2. *Quaternary Science Reviews* **25**, 3150–3184.

Ding, Z.L., Derbyshire, E., Yang, S.L., Sun, J.M., Liu, T.S., 2005. Stepwise expansion of desert environment across northern China in the past 3.5 Ma and implications for monsoon evolution. *Earth and Planetary Science Letters* **237**, 45–55.

Ding, Z.L., Ranov, V., Yang, S.L., Finaev, A., Han, J.M., Wang, G.A., 2002. The loess record in southern Tajikistan and correlation with Chinese loess. *Earth and Planetary Science Letters* **200**, 387–400.

Duan, Z., Hu, W., 2001. The accumulation of potash in a continental basin: the example of the Qarhan saline lake, Qaidam Basin, West China. *European Journal of Mineralogy* **13**, 1223–1233.

Dupont-Nivet, G., Krijgsman, W., Langereis, C.G., Abels, H.A., Dai, S., Fang, X., 2007. Tibetan Plateau aridification linked to global cooling at the Eocene–Oligocene transition. *Nature* **445**, 635–638.

Evans, M.E., Heller, F., 2003. *Environmental Magnetism: Principles and Applications of Enviromagnetics*. Academic Press, New York.

Fang, X., An, Z., Clemens, S., Zan, J., Shi, Z., Yang, S., Han, X., 2020. The 3.6-Ma aridity and westerlies history over mid-latitude Asia linked with global climatic cooling. *Proceedings of the National Academy of Sciences* **117**, 24729–24734.

Fang, X., Galy, A., Yang, Y., Zhang, W., Ye, C., Song, C., 2019. Temperature forcing paleogene chemical weathering intensity in the northern Tibet Plateau. *Geology* **47**, 992–996.

Fang, X., Li, J., Van der Voo, R., 1999. Rock magnetic and grain size evidence for intensified Asian atmospheric circulation since 800,000 years B.P. related to Tibetan uplift. *Earth and Planetary Science Letters* **165**, 129–144.

Fang, X., Shi, Z., Yang, S., Yan, M., Li, J., Jiang, P., 2002. Loess in the Tian Shan and its implications for the development of the Gurbantunggut Desert and drying of northern Xinjiang. *Chinese Science Bulletin* **47**, 1381–1387.

Felzer, B., Oglesby, R.J., Hong, S., Iii, T.W., Hyman, D.E., Prell, W.L., Kutzbach, J.E., 1995. A systematic study of GCM sensitivity to latitudinal changes in solar radiation. *Journal of Climate* **8**, 877–887.

Gradstein, F., Ogg, J., Schmitz, M., Ogg, G., 2012. *The Geologic Time Scale 2012*. Amsterdam, Netherlands: Elsevier.

Gu, S., Xu, W., Xue, C., Di, S., Yang, F., Di, H., Zhao, D., 1990. *Regional Petroleum Geology of Qinghai-Xizang Oil-Gas Field*. [In Chinese.] Petroleum Publishing House, Beijing.

Guo, P., Liu, C., Huang, L., Yu, M., Wang, P., Zhang, G., 2018. Palaeohydrological evolution of the Late Cenozoic saline lake in the Qaidam Basin, NE Tibetan Plateau: tectonic vs. climatic control. *Global and Planetary Change* **165**, 44–61.

Guo, Z.T., Ruddiman, W.F., Hao, Q.Z., Wu, H.B., Qiao, Y.S., Zhu, R.X., Peng, S.Z., Wei, J.J., Yuan, B.Y., Liu, T.S., 2002. Onset of Asian desertification by 22 Myr ago inferred from loess deposits in China. *Nature* **416**, 159–163.

Han, W., Fang, X., Berger, A., 2012. Tibet forcing of mid-Pleistocene synchronous enhancement of East Asian winter and summer monsoons revealed by Chinese loess record. *Quaternary Research* **78**, 174–184.

Han, W., Fang, X., Ye, C., Teng, X., Zhang, T., 2014. Tibet forcing Quaternary stepwise enhancement of westerly jet and central Asian aridification: carbonate isotope records from deep drilling in the Qaidam salt playa, NE Tibet. *Global and Planetary Change* **116**, 68–75.

Han, W., Ma, Z., Lai, Z., Appel, E., Fang, X., Yu, L., 2013. Wind erosion on the north-eastern Tibetan Plateau: constraints from OSL and U-Th dating of playa salt crust in the Qaidam Basin. *Earth Surface Processes and Landforms* **39**, 779–789.

Huang, H.C., Huang, Q.H., Ma, Y.S., 1996. Geology of Qaidam Basin. In: Huang, H.C., *Geology of Qaidam and Its Petroleum Prediction*. [In Chinese.] Geological Publishing House, Beijing, pp. 1–88.

Kapp, P., Pelletier, J.D., Rohrmann, A., Heermance, R., Russell, J., Ding, L., 2011. Wind erosion in the Qaidam Basin, central Asia: implications for tectonics, paleoclimate, and the source of the Loess Plateau. *GSA Today* **21**, 4–10.

Kutzbach, J.E., Guetter, P.J., Ruddiman, W.F., Prell, W.L., 1989. Sensitivity of climate to Late Cenozoic uplift in southern Asia and the American West: numerical experiments. *Journal of Geophysical Research* **94**, 18393–18407.

Kutzbach, J.E., Prell, W.L., Ruddiman, W.F., 1993. Sensitivity of Eurasian climate to surface uplift of the Tibetan Plateau. *The Journal of Geology* **101**, 177–190.

Laj, C., Channell, J.E.T., 2007. Geomagnetic excursions. In: Kono, M. (Ed.), *Geomagnetism Treatise on Geophysics* 5, Elsevier, Amsterdam, pp. 373–416.

Langereis, C.G., Dekkers, M.J., Lange, G.J., Paterne, M., Santvoort, P.J.M., 1997. Magnetostratigraphy and astronomical calibration of the last 1.1 Myr from an eastern Mediterranean piston core and dating of short events in the Brunhes. *Geophysical Journal International* **129**, 75–94.

Li, J., Li, M., Fang, X., Zhang, G., Zhang, W., Liu, X., 2017. Isotopic composition of gypsum hydration water in deep Core SG-1, western Qaidam Basin (NE Tibetan Plateau): implications for paleoclimatic evolution. *Global and Planetary Change* **155**, 70–77.

Lisiecki, L.E., Raymo, M.E., 2005. A Pliocene–Pleistocene stack of 57 globally distributed benthic $\delta^{18}O$ records. *Paleoceanography and Paleoclimatology* **20**, 522–533.

Liu, D., Fang, X., Gao, J., Wang, Y., Zhang, W., Miao, Y., Liu, Y., Zhang, Y., 2009. Cenozoic stratigraphy deformation history in the central and eastern of Qaidam Basin by the balance section restoration and its implication. *Acta Geologica Sinica* **83**, 359–371.

Lu, Y., Fang, X., Appel, E., Wang, J., Herb, C., Han, W., Wu, F., Song, C., 2015. A 7.3–1.6 Ma grain size record of interaction between anticline uplift and climate change in the western Qaidam Basin, NE Tibetan Plateau. *Sedimentary Geology* **319**, 40–51.

Lü, L., Fang, X., Mason, J.A., Li, J., An, Z., 2001. The evolution of coupling of Asian winter monsoon and high latitude climate of Northern Hemisphere. *Science in China Series D: Earth Sciences* **44**, 185–191.

Lund, S., Stoner, J.S., Channell, J.E.T., Acton, G., 2006. A summary of Brunhes paleomagnetic field variability recorded in Ocean Drilling Program cores. *Physics of the Earth and Planetary Interiors* **156**, 194–204.

Maher, B.A., 1988. Magnetic properties of some synthetic submicron magnetite. *Geophysical Journal International* **94**, 83–96.

Molnar, P., England, P., Martinod, J., 1993. Mantle dynamics, uplift of the Tibetan Plateau, and the Indian monsoon. *Reviews of Geophysics* **31**, 357–396.

Mudelsee, M., Schulz, M., 1997. The mid-Pleistocene climate transition: onset of 100 ka cycle lags ice volume build-up by 280 ka. *Earth and Planetary Science Letters* **151**, 117–123.

Ramstein, G., Fluteau, F., Besse, J., Joussaume, S., 1997. Effect of orogeny, plate motion and land sea distribution on Eurasian climate change over the past 30 million years. *Nature* **386**, 788–795.

Raymo, M.E., Ruddiman, W.F., 1992. Tectonic forcing of Late Cenozoic climate. *Nature* **359**, 117–122.

Roberts, A.P., Cui, Y., Verosub, K.L., 1995. Wasp-waisted hysteresis loops: mineral magnetic characteristics and discrimination of components in mixed magnetic systems. *Journal of Geophysical Research: Solid Earth* **100**, 17909–17924.

https://doi.org/10.1017/qua.2021.15 Published online by Cambridge University Press

Ruddiman, W.F., Kutzbach J.E., 1989. Forcing of Late Cenozoic Northern Hemisphere climate by plateau uplift in southern Asia and the American West. *Journal of Geophysical Research* **94**, 18409–18427.

Ruddiman, W.F., Raymo, M.E., Martinson, D.G., Clement, B.M., Backman, J., 1989. Pleistocene evolution: Northern Hemisphere ice sheets and North Atlantic Ocean. *Paleoceanography* **4**, 353–412.

Schmieder, F., von Dobeneck, T., Bleil, U., 2000. The mid-Pleistocene climate transition as documented in the deep South Atlantic Ocean: initiation, interim state and terminal event. *Earth and Planetary Science Letters* **179**, 539–549.

Shen, Z., Cheng, G., Le, C., 1993. Magnetostratigraphy and chronostratigraphy. In: Shen, Z., *The Division and Sedimentary Environment of Quaternary Salt-Bearing Strata in Qaidam Basin*. [In Chinese.] Geological Publishing House, Beijing, pp. 30–166.

Shi, L., Zheng, M., Li, J., Wang, Y., Hou, X., Ma N., 2010. Magnetostratigraphy of Liang ZK05 borehole in Dalangtan, Qaidam Basin. [In Chinese.] *Acta Geologica Sinica* **84**, 1631–1640.

Song, Y., Fang, X., King, J.W., Li, J., Naoto, I., An, Z., 2014. Magnetic parameter variations in the Chaonaloess/paleosol sequences in the central Chinese Loess Plateau, and their significance for the middle Pleistocene climate transition. *Quaternary Research* **81**, 433–444.

Song, Y., Luo, D., Du, J., Kang, S., Cheng, P., Fu, C., Guo, X., 2018. Radiometric dating of late Quaternary loess in the northern piedmont of South Tianshan Mountains: implications for reliable dating. *Geological Journal* **53**, 417–426.

Su, Q., Nie, J., Meng, Q., Heermance, R., Gong, L., Luo, Z., Wang, Z., Zhang, R., Garzione, C., 2019. Central Asian drying at 3.3 Ma linked to tropical forcing? *Geophysical Research Letters* **46**. https://doi.org/10.1029/2019GL084648.

Sun, J., Liu, T., 2006. The age of the Taklimakan Desert. *Science* **312**, 1621.

Tan, M., Zhang, W., Fang, X., Yan, M., Zan, J., Zhang, T., 2020. Rock magnetic record of core SG-3 since 1 Ma in the western Qaidam Basin and its paleoclimate implications for the NE Tibetan Plateau. *Palaeogeography, Palaeoclimatology, Palaeoecology* **560**. https://doi.org/10.1016/j.palaeo.2020.10994.

Thompson, R., Oldfield, F., 1986. *Environmental Magnetism*. Allen and Unwin, London.

Thouveny, N., Bourlès, D.L., Saracco, G., Carcaillet, J., Bassinot, F., 2008. Paleoclimatic context of geomagnetic dipole lows and excursions in the Brunhes: clue for an orbital influence on the geodynamo? *Earth and Planetary Science Letters* **275**, 269–284.

Wang, E., Burchfiel, B.C., 2004. Late Cenozoic right lateral movement along the Wenquan Fault and its implications for the kinematics of the Qaidam Basin, the northeastern margin of the Tibetan Plateau. *International Geology Review* **46**, 861–879.

Wang, E., Xu, F., Zhou, J., Wan, J., Burchfiel, B. C., 2006. Eastward migration of the Qaidam Basin and its implications for Cenozoic evolution of the Altyn Tagh Fault and associated river systems. *Geological Society of America Bulletin* **118**, 349–365.

Wang, J., Fang, X., Appel E., Song, C., 2012. Pliocene–Pleistocene climate change at the NE Tibetan Plateau deduced from lithofacies variation in the drill core SG-1, western Qaidam Basin, China. *Journal of Sedimentary Research* **82**, 933–952.

Wang, J., Fang, X., Appel, E., Zhang, W., 2013. Magnetostratigraphic and radiometric constraints on salt formation in the Qaidam Basin, NE Tibetan Plateau. *Quaternary Science Reviews* **78**, 53–64.

Wang, J., Wang, Y., Liu, Z., Li, J., Xi, P., 1999. Cenozoic environmental evolution of the Qaidam Basin and its implications for the uplift of the Tibetan Plateau and the drying of central Asia. *Paleogeography, Paleoclimatology, Paleoecology* **152**, 37–47.

Wu, F., Fang, X., Ma, Y., Herrmann, M., Mosbrugger, V., An, Z., Miao, Y., 2007. Plio-Quaternary stepwise drying of Asia: evidence from a 3-Ma pollen record from the Chinese Loess Plateau. *Earth and Planetary Science Letters* **257**, 160–169.

Xia, W., Zhang, N., Yuan, X., Fan, L., Zhang, B., 2001. Cenozoic Qaidam Basin, China: a stronger tectonic inversed, extensional rifted basin. *American Association of Petroleum Geologist Bulletin* **85**, 715–736.

Yang, L., Zhang, W., Fang, X., Cai, M., Lu, Y., 2020b. Aridification recorded by lithofacies and grain size in a continuous Pliocene–Quaternary lacustrine sediment record in the western Qaidam Basin, NE Tibetan Plateau. *Palaeogeography, Palaeoclimatology, Palaeoecology* **556**. https://doi.org/10.1016/j.palaeo.2020.109903.

Yang, S., Li, D., Liu, N., Zan, J., Liu, W., Kang, J., Murodov, A., Fang, X., 2020a. Quartz optically stimulated luminescence dating of loess in Tajikistan and its paleoclimatic implications for arid central Asia since the Late Glacial. *Palaeogeography, Palaeoclimatology, Palaeoecology* **556**. https://doi.org/10.1016/j.palaeo.2020.109881.

Yang, Y., Fang, X., Appel, E., Galy, A., Li, M., Zhang, W., 2013. Late Pliocene–Quaternary evolution of redox conditions in the western Qaidam paleolake (NE Tibetan Plateau) deduced from Mn geochemistry in the drilling core SG-1. *Quaternary Research* **80**, 586–595.

Yang, Y., Fang, X., Koutsodendris, A., Ye, C., Yang, R., Zhang W., Liu, X., Gao S., 2016. Exploring Quaternary paleolake evolution and climate change in the western Qaidam Basin based on the bulk carbonate geochemistry of lake sediments. *Palaeogeography, Palaeoclimatology, Palaeoecology* **446**, 152–161.

Yin, A., Dang, Y., Zhang, M., Chen, X., McRivette, M.W., 2008. Cenozoic tectonic evolution of the Qaidam Basin and its surrounding regions (part 3): structural geology, sedimentation, and regional tectonic reconstruction. *Geological Society of America Bulletin* **120**, 847–876.

Yin, A., Rumelhart, P.E., Bulter, R., Cowgill, E., Harrison, T.M., Foster, D.A., Ingersoll, R.V., *et al.*, 2002. Tectonic history of the Altyn Tagh Fault system in northern Tibet inferred from Cenozoic sedimentation. *Geological Society of America Bulletin* **114**, 1257–1295.

Yuan, J., Huo, C., Cai, K., 1983. The high mountain-deep basin saline environment: a new genetic model of salt deposits. [In Chinese with English abstract.] *Geological Review* **29**, 159–165.

Zan, J., Fang, X., Li, X., Zhang, W., Yan, M., Shen, M., 2018. Late Pliocene monsoonal rainfall gradients in western China recorded by the eolian deposits from the Linxia Basin, NE Tibetan Plateau. *Journal of Geophysical Research: Atmospheres* **123**, 8047–8061.

Zan, J., Fang, X., Yang, S., Nie, J., Li, X., 2010. A rock magnetic study of loess from the West Kunlun Mountains. *Journal of Geophysical Research* **115**, B10101. https://doi.org/10.1029/2009JB007184.

Zan, J., Fang, X., Yang, S., Yan, M., 2013. Evolution of the arid climate in High Asia since ~1 Ma: evidence from loess deposits on the surface and rims of the Tibetan Plateau. *Quaternary International* **313–314**, 210–217.

Zhang, W., Appel, E., Fang, X., Setzer, F., Song, C., Meng, Q., Yan, M., 2020. New paleomagnetic constraints on syntectonic growth strata in the western Qaidam Basin, NE Tibetan Plateau. *Tectonophysics* **780**. https://doi.org/10.1016/j.tecto.2020.228401.

Zhang, W., Appel, E., Fang, X., Song, C., Cirpka, O., 2012a. Magnetostratigraphy of deep drilling core SG-1 in the western Qaidam Basin (NE Tibetan Plateau) and its tectonic implications. *Quaternary Research* **78**, 139–148.

Zhang, W., Appel, E., Fang, X., Song, C., Setzer, F., Herb, C., Yan, M., 2014. Magnetostratigraphy of drill-core SG-1b in the western Qaidam Basin (NE Tibetan Plateau) and tectonic implications. *Geophysical Journal International* **197**, 90–118.

Zhang, W., Appel, E., Fang, X., Yan, M., Song, C., Cao, L., 2012b. Paleoclimatic implications of magnetic susceptibility in Late Pliocene–Quaternary sediments from deep drilling core SG-1 in the western Qaidam Basin NE Tibetan Plateau. *Journal of Geophysical Research: Solid Earth* **117**, B06101. https://doi.org/10.1029/2011JB008949.

Zhang, W., Fang, X., Song, C., Appel, E., Yan, M., Wang, Y., 2013. Late Neogene magnetostratigraphy in the western Qaidam Basin (NE Tibetan Plateau) and its constraints on active tectonic uplift and progressive evolution of growth strata. *Tectonophysics* **599**, 107–116.

Zhou, J., Xu F., Wang, T., Gao, A., Yin, C., 2006. Cenozoic deformation history of the Qaidam Basin, NW China: results from cross-section restoration and implications for Qinghai–Tibet Plateau tectonics. *Earth and Planetary Science Letters* **243**, 195–2l0.

https://doi.org/10.1017/qua.2021.15 Published online by Cambridge University Press